Bull. Mater. Sci., Vol. 17, No. 5, October 1994, pp. 513–522. © Printed in India.

Origin of visible photoluminescence from porous silicon as studied by Raman spectroscopy

A ROY†, K JAYARAM and A K SOOD*
Department of Physics and †Solid State and Structural Chemistry Unit, Indian Institute of Science, and *Jawaharlal Nehru Centre for Advanced Scientific Research, Bangalore 560012, India

Abstract. In this paper we discuss the different models proposed to explain the visible luminescence in porous silicon (PS). We review our recent photoluminescence and Raman studies on PS as a function of different preparation conditions and isochronal thermal annealing. Our results can be explained by a hybrid model which incorporates both nanostructures for quantum confinement and silicon complexes (such as SiH_x and siloxene) and defects at Si/SiO_2 interfaces as luminescent centres.

Keywords. Porous silicon; nanoparticles; photoluminescence; Raman spectroscopy.

1. Introduction

The recent observations of highly efficient visible photo- and electroluminescence at room temperature from electrochemically etched porous silicon (PS) have stimulated a lot of excitement because of its possible use in optoelectronic applications. The formation of PS was first reported about 38 years ago by Uhlir (1956) during electropolishing of silicon in aqueous HF solution. Interest in PS was revived when Canham (1990) suggested that the origin of visible photoluminescence (PL) involves quantum size effects on the electronic states in quantum wires (of diameter < 50 Å) of crystalline silicon formed due to decrease in the dimension of the silicon pore walls. Later it was suggested that the PL in PS could arise due to the formation of silicon-based compounds like SiH_x (Friedersdorf *et al* 1992) or siloxene (Brandt *et al* 1992) or siloxene-like derivatives (Roy *et al* 1992). Till today the origin of visible PL in PS is very much controversial. In this paper we review the known theoretical models in light of our own work on Raman and PL studies. §2 summarizes the models proposed to explain the visible PL, §3 discusses briefly the experimental details and §4 contains our main experimental observations and their discussion based on the hybrid model.

2. Models

2.1 *Quantum confinement model*

In quantum confinement model, anodization of Si wafer in HF or HF-ethanol electrolyte at low current densities generates nanostructured 'Si-wires' separated by holes. Transmission electron microscopy has been used to support this idea (Cullis and Canham 1991). These nanostructures have larger band gap than bulk silicon due to quantum confinement. The radiative recombination of electrons and holes, generated by the incident radiation, occurs in these nanoparticles giving rise to PL in

the visible range. Electronic structures of hydrogen-terminated Si-wires (diameter 30 – 100 Å) based on density functional theory with local density approximation (Buda *et al* 1992) and first-principle pseudopotential calculation (Read *et al* 1992) have shown that these structures have direct band gap at the zone centre of magnitude ~ 1·5 to 2 eV, accounting for the high PL efficiency in the visible range. It has been found that the observed PL peak energies as a function of electrolyte composition and time of etching do not vary continuously but have discrete values (Wang *et al* 1993). This behaviour has been explained by the fact that the anodic etching of Si in HF solutions results in formation of closed-shell silicon structures of specific diameters for which the band gaps, calculated by tight binding approximation, have only discrete values.

Some of the experimental results on PS explained by the above model are as follows: (i) During rapid thermal oxidation (RTO) hydrogen desorbs from the surface of the PS; dangling bond gets saturated by oxygen and forms SiO_2 which surrounds small crystalline regions and protects these small regions from further oxidation. Hence the stability of PL and cathodoluminescence is more stable for RTO samples than for as-prepared ones (Batstone *et al* 1993). (ii) The blue or red shift in PL after HF vapour etching is due to changes in the size of the particles (Shih *et al* 1993). (iii) The asymmetry in the first-order Raman Si line for PS towards low frequency can be explained due to confinement of phonons in these nanoparticles (Sui *et al* 1992). (iv) The experimental decay time of visible photoluminescence in PS is between 10 μs and 1 ms (Vial *et al* 1992). Such a long lifetime is more compatible with the hypothesis of quantum confinement in silicon crystallites (diameter > 10 Å) (Proot *et al* 1992).

2.2 *Photoluminescence extrinsic to Si: silicon derivatives based models*

It has been suggested that the anodic etching of p-doped Si wafer results in formation of siloxene ($Si_6O_3H_6$) and siloxene derivatives which are responsible for visible PL. A detailed study of PL, infrared (IR) and Raman spectroscopic measurements have been carried out in siloxene (both Kautsky siloxene and Wöhler siloxene) and PS (Fuchs *et al* 1993). The influence of thermal annealing, chemical treatment or laser radiation on vibrational spectra and X-ray diffraction pattern of siloxene and PS have been shown to be similar. In particular, Raman and IR transmission spectra are almost alike over the entire frequency range from 300 cm^{-1} to 4000 cm^{-1}. The ratio of Si to O in PS measured by X-ray photoelectron spectroscopy (XPS) is 2:1 (Roy *et al* 1992). Within the possibility of existence of hydrogen (which cannot be seen by XPS), it has been proposed that PS contains fluorine-substituted siloxene derivative.

Siloxene and its derivatives have outstanding luminescence properties. The structure of as-prepared siloxene consists of the layers of $[Si_2H(OH)]_{3n}$ or $[Si_2H_2O]_{3n}$ or $[Si_2H_6O_3]_n$. Each of these layers consists of a regular array of oxygen atoms which isolate quantum wires and/or quantum dots in silicon and the remaining dangling bonds are saturated by monovalent radicals like hydrogen. Electronic structure of such structures using semi-empirical quantum calculation predicts optical properties which fit well with those of PS (Deák *et al* 1992).

IR spectrum of PS shows bands at 900 cm^{-1}, corresponding to scissor mode of SiH_2 and at 666 cm^{-1} and 621 cm^{-1} which can be attributed to deformation modes

of SiH and SiH_2 respectively (Weng *et al* 1993). These observations point out to the formation of SiH_x in PS.

2.3 *Formation of the defect states*

Defect states formed during formation of PS have been considered as luminescent centres. The observation of the PL spectral shifts with the composition of electrolyte and post-etching treatments in different chemical solvents suggests that the PL is related to the surface states of PS. For example, the PL is peaked at 2·4 eV when H_2O: 49% HF (3:1) or H_2O:acetic acid:49% HF (2:1:1) is used as electrolyte (Li *et al* 1993) whereas for HF:ethyl alcohol (1:1) electrolyte the PL peak energy is at 1·73 eV (Roy *et al* 1994).

2.4 *Hybrid model*

A model which incorporates both nanostructure and silicon derivatives and defect states has been proposed (Qin and Jia 1993). According to this model the incident radiation creates the electron – hole pair in the nanoscale structures present in PS but unlike in quantum confinement model they do not recombine radiatively inside the nanoparticles. Instead, they diffuse out and recombine at various luminescent centres which can be defect states at Si/SiO_2 interfaces or silicon complexes like SiH_x/silōxene at the surfaces of the nanoparticles.

3. Experimental

The porous silicon was prepared by anodic etching of boron-doped p-type Si wafers of ⟨100⟩ orientation (resistivity ~ 1 Ω-cm). To study the correlation between the PL and Raman spectra of PS, a large number of PS samples were prepared with different experimental conditions (Sood *et al* 1992). Here we report the preparation condition, current densities, time of etching and electrolytes used for four such samples:sample A, 15 mA/cm^2 for 30 min in 20% aqueous HF solution; sample B, 15 mA/cm^2 for 40 min in 48% aqueous HF solution; sample C, 35 mA/cm^2 for 20 min followed by 7 mA/cm^2 for 20 min in 10% aqueous HF solution; and sample D, 15 mA/cm^2 for 30 min in 10% aqueous HF solution. To study the effect of thermal annealing on PS, the sample was prepared in 48% HF:ethanol (1:1) solution, keeping the current density between 10 and 15 mA/cm^2. PL and Raman spectra were recorded at room temperature in 45° reflection geometry using the 5145 Å line of an argon ion laser as excitation source and a computer-controlled SPEX Ramalog (model 14018) equipped with a cooled photomultiplier tube and a photon counting system. For thermal treatment in air, the sample was introduced in the temperature-controlled furnace maintained at a desired annealing temperature (T_a) and kept for 5 min. Then it was taken out of the furnace and cooled to room temperature to record both Raman and PL spectra at the same spot of the sample. The sample was annealed at seventeen different temperatures ranging from 25°C to 900°C with interval of 50°C. The experiments were repeated on three samples to check reproducibility of the results.

4. Results and discussion

4.1 *Correlation between PL and Raman spectra*

It is known that the Raman line in nanoparticles of Si shifts to lower frequencies and is asymmetric due to phonon confinement (Richter *et al* 1981). If the observed PL is associated with the band-to-band recombination in the nanoparticles, the blue shift in PL is expected to be correlated with the red shift in the Raman peak position with respect to crystalline silicon (c-Si). Such a correlation was reported by Tsu *et al* (1992). In contrast, our similar study on a large number of samples prepared using different electrolytes, current densities and time of etching does not show such a correlation (Sood *et al* 1992). Figure 1 shows PL spectra of four different samples. The corresponding Raman spectra are shown in figure 2 where the Raman line of c-Si is shown by a dashed line. The current density, electrolyte and time of etching for the preparation of the four samples have been discussed in § 3. From the above figures it is obvious that there is no correlation between blue shifts in PL peak energy and red shift in Raman phonon line. Sample D has the highest PL peak position whereas the Raman line shows lower red shift than sample A where the PL is peaked at lower energy. The clear absence of correlation goes against the confinement model.

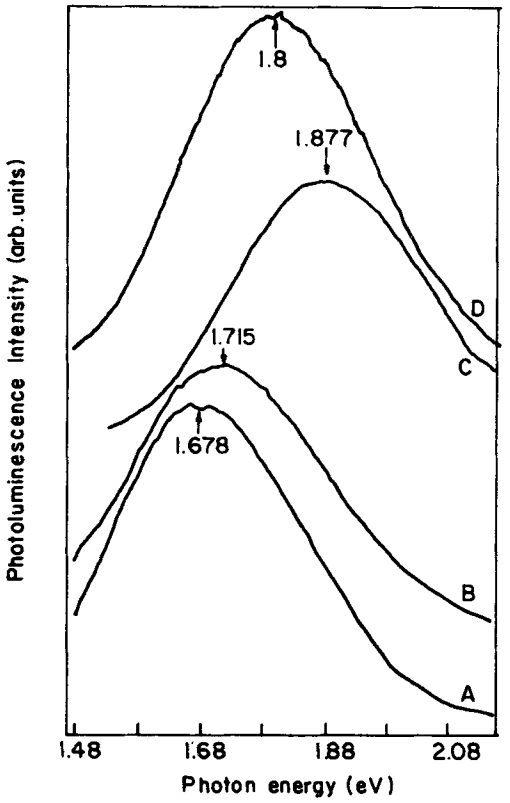

Figure 1. Photoluminescence spectra of four different samples of porous silicon A, B, C and D. (See § 3 for details of the sample preparation).

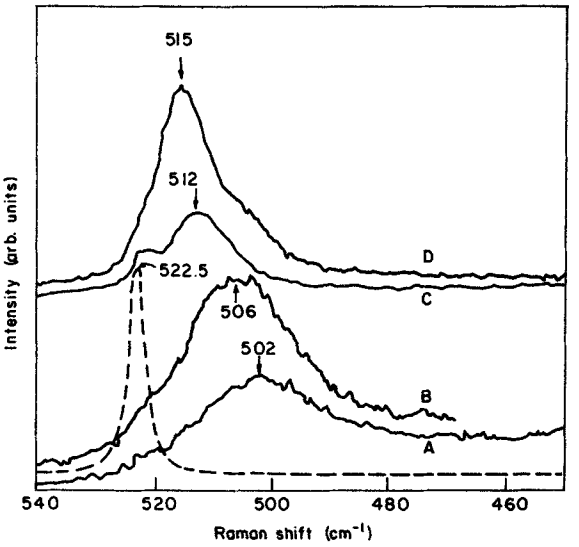

Figure 2. Raman spectra corresponding to the photoluminescence spectra of figure 1 for different samples. The dotted line is the Raman spectrum of crystalline silicon.

4.2 *PL and Raman spectroscopic studies in thermally annealed PS*

Isochronal thermal annealing studies (annealing temperature T_a varied from room temperature to 900°C with a step of 50°C) were carried out to understand the influence of hydrogen desorption from the surface of PS at 350°C and repassivation by oxygen at higher annealing temperatures (Roy *et al* 1994). Figure 3a shows the PL of PS at nine different temperatures. The intensity scale in the figure is the same for all spectra and hence one can clearly see the nonmonotonic variation of intensity of PL with temperature. The measured PL spectra are fitted by nonlinear least-square fitting using Gaussian profile. The variation of PL peak positions and intensities (area under the band) as a function of annealing temperature T_a is shown in figures 4a and b. The solid lines in figure 4 have been drawn through the points as guides to the eye. It can be seen from figure 4a that the PL peak energy is 1·73 eV in as-prepared PS and increases to 1·77 eV at $T_a = 100$°C and then gradually red-shifts to 1·68 eV at $T_a = 600$°C. Above 600°C the peak energy increases and recovers to 1·74 eV ($T_a = 750$°C). In figure 4b we see that the PL intensity remains constant till T_a reaches 100°C and then it increases up to $T_a = 350$°C, followed by a decrease. Above 550°C the intensity of PL from PS again starts increasing and then decreases for $T_a > 650$°C. At 800°C, the PL vanishes completely.

The corresponding changes in Raman spectra as a function of annealing temperature are shown in figure 3b. The Raman spectrum of *c*-Si has been shown in the same figure (top curve). The Raman line of PS is red-shifted and highly asymmetric till $T_a = 550$°C. It is known that the asymmetric Raman line shape can arise due to phonon confinement in the nanoscale crystallites (Richter *et al* 1981; Campbell and Fauchet 1986). In this model the Raman line shape is given by

$$I_c(\omega) = A \int_0^{q_{max}} \frac{d\vec{q}|c(0,\vec{q})|^2}{[\omega - \omega(\vec{q})]^2 + [\Gamma_c/2]^2},$$

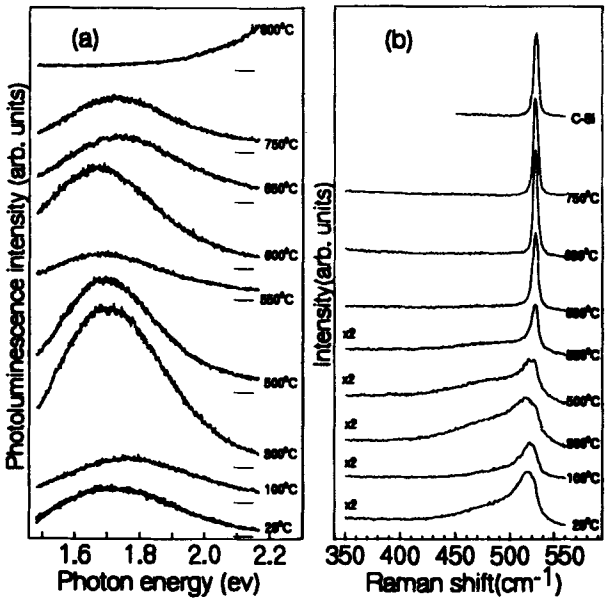

Figure 3. **(a)** Photoluminescence spectra of porous silicon at nine different annealing temperatures. Intensity scale is the same for all spectra. The horizontal line on the right of each spectrum shows the zero of the intensity scale. **(b)** Raman spectra of porous silicon at eight different annealing temperatures. The Raman line of bulk crystalline Si is shown at the top.

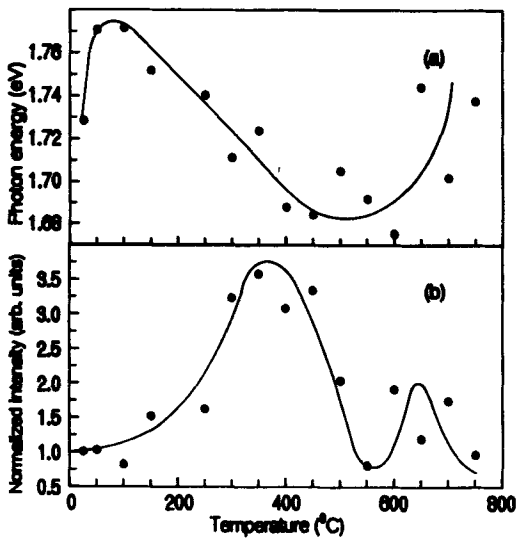

Figure 4. Variation of the photoluminescence **(a)** peak position and **(b)** intensity of porous silicon as a function of annealing temperature. The intensities are normalized with respect to that of as-prepared porous silicon. The solid lines through the data points are guides to the eye.

where $\omega(\vec{q})$ is the phonon dispersion curve for bulk silicon, which has been taken as $\omega(\vec{q}) = \omega_0(1 - 0{\cdot}18\,q^2)$, which fits the experimental curve well in the direction of $\Gamma - X$ up to $q = 0{\cdot}8$. ω_0 and Γ_c are phonon frequency ($\vec{q} = 0$) and the natural linewidth of the bulk silicon, the values of which have been taken as $\omega_0 = 521{\cdot}9\,\mathrm{cm}^{-1}$ and $\Gamma_c = 4{\cdot}7\,\mathrm{cm}^{-1}$. The wavevector q has been expressed in units of $2\pi/a$ (where a is the lattice constant of Si = 5·4 Å) and $q_{\max} = 0{\cdot}8$. A is a constant. $c(0, \vec{q})$ is the Fourier coefficient of the phonon confinement function. One may note that the Raman line in nanoparticles is red-shifted and asymmetric towards the low-frequency side because the phonon dispersion $\omega(\vec{q})$ in bulk silicon is a decreasing function of q. We have used the phonon confinement function to be Gaussian which is found to be suitable for microcrystalline Si: $|c(0, \vec{q})|^2 = \exp[-q^2L^2/(4a^2)]$, where L is the dimension of the nanocrystallite of Si (equal to diameter of the cylinder for infinitely long cylindrical particles and equal to diameter for spherical particles). It has been shown that for PS the phonon confinement in spherical particles explains the line shape better than with cylindrical shapes (Sood *et al* 1992; Sui *et al* 1992). We have tried to fit the experimental Raman spectra for PS using the above model with spherical particles with diameter L. The best fit with diameter $L = 42{\cdot}7$ Å is shown by a dashed line in figure 5 for as-prepared PS. It is obvious from figure 5 that the phonon confinement model alone fails to explain the PS Raman line shape.

It has been reported that the PL peak energy decreases whereas intensity increases as the sampling spot is moved towards the edge of the sample (Lee *et al* 1993). It has also been shown that the Raman peak position of the inner sampling spot is the same as that in *c*-Si; intensity of *c*-Si peak decreased and another peak at about $500\,\mathrm{cm}^{-1}$ increased as the sampling spot moved towards the edge of the sample. The above experimental result is explained by the fact that during anodic dissolution, there is a deposition of silicon atoms on the top of the surface layers. The deposition is more towards the edge of the sample. The redeposited Si is a mixture of microcrystalline phase and amorphous phase and both of these phases contribute to increase in PL intensity at the edge of the PS sample. The deposition of amorphous Si phase also explains the gradual increase in Raman line intensity at $500\,\mathrm{cm}^{-1}$ as the sampling spot is moved towards the edge of the sample. In addition, Raman scattering measurements of microcrystalline silicon prepared in hydrogen plasma have shown crystalline as well as amorphous features. The latter has been attributed to a surface-like Si – Si shearing mode at the grain boundaries of the microcrystallites (Iqbal and Vepřek 1982).

Keeping in mind the possibility of the presence of disordered/amorphous silicon together with the crystalline nanoparticles, we attempted to fit the observed line shape with a combined line shape

$$I(\omega) = I_c(\omega) + I_d(\omega),$$

where

$$I_d(\omega) = B\Gamma_d[(\omega - \omega_d)^2 + \Gamma_d^2]^{-1},$$

is the Lorenzian line shape and arises due to the disordered/amorphous component of the PS. Here ω_d and Γ_d are the phonon frequency and half width at half maximum (HWHM) respectively for the disordered component and B is a constant. We have carried out nonlinear least-square fit of the data with $I(\omega)$, keeping L, ω_d, Γ_d, A and B as fitting parameters. In figure 5 we have plotted the fitted $I(\omega)$ (solid line), and it

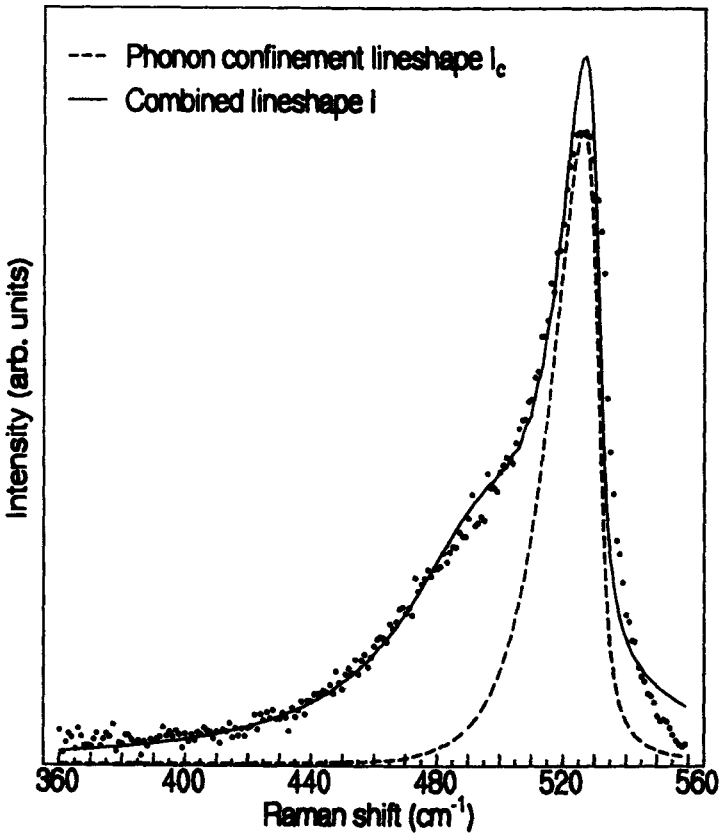

Figure 5. Dots show the Raman spectrum of as-prepared porous silicon. The dashed line shows the fit using the confinement model alone $I_c(\omega)$. The solid line shows the best fit using $I_c(\omega) + I_d(\omega)$ (sum of phonon confinement effect and disordered component).

is obvious from this figure that the combined Raman line shape $I(\omega)$ fits extremely well with the experimental spectrum. In figure 6 we show the variation in relative intensity B/A of the two components $I_d(\omega)$ and $I_c(\omega)$ with different T_a. The solid line through the points is a guide to the eye.

Our experimental results can be explained in terms of the new hybrid model (Qin and Jia 1993). Initial increase in PL intensity with annealing temperature in figure 4b suggests an increase in defect density during thermal annealing. As PS is heated beyond 350°C, hydrogen desorbs from the sample as seen in EPR studies (via increase in dangling bonds) (Bhat *et al* 1992) and infrared absorption measurements (Prokes *et al* 1992). This will decrease the defects related to Si – H complexes at the surface of the nanostructures and hence PL intensity. This can also cause a decrease in PL peak position. Further heating ($T_a > 500$°C) results in repassivation of the dangling bonds due to formation of SiO_2. These newly formed defect states at Si/SiO_2 interface or the defects in SiO_2 again increase PL intensity and can also result in higher PL peak position as seen in figure 4a. Now, coming to Raman scattering results, we note the following: Variation of the relative intensity (B/A) [intensity of $I_d(\omega)$/intensity of

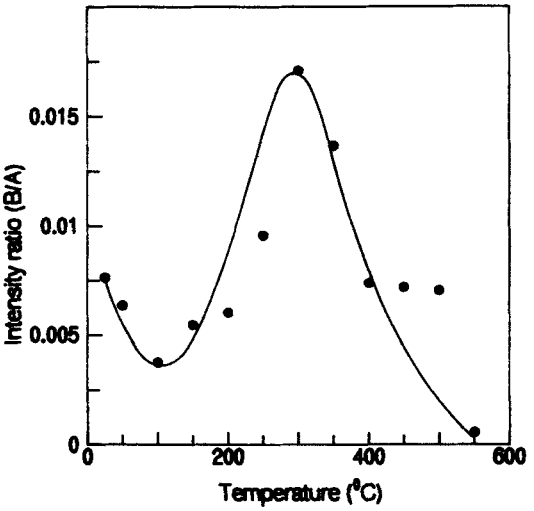

Figure 6. Variation of the relative intensity of two components of Raman line, B/A, with different annealing temperatures. The solid line through the points is a guide to the eye.

$I_c(\omega)$] in figure 6 agrees with the above conclusion that the disorder in the form of possible Si – H complexes first increases up to 350°C and then decreases. The drastic change in the Raman line shape for $\Gamma_a > 550$°C can arise because increasing portions of nanoscale Si get converted into SiO_2. As SiO_2 has much lower absorption coefficient for the incident radiation at 2·41 eV (as observed in the shift of the absorption band at $T_a \sim 600$°C (Petrova-Koch *et al* 1992)) the Raman signal will be dominated by the underlying substrate.

Results shown in figures 1 and 2 can also be rationalized on the basis of the hybrid model because the preparation conditions decide the preponderance of certain types of defects which are not linked with the size of the nanoparticles responsible for the red shift of the Raman line.

5. Conclusions

(i) There is no direct correlation between the blue shift in PL and the red shift in Raman spectra of PS. (ii) The quantum confinement model or the models which propose the formation of Si-based compounds or defect states are individually not sufficient to explain the visible PL in PS. (iii) A hybrid model which incorporates the features of nanoscale units acting as a reservoir of the electron – hole pairs and silicon complexes (with O, H and F) and defects located outside the nanoparticles as radiative luminescent centres can explain our experimental results reasonably well. More spectroscopic and structural studies are required to sharpen our understanding of porous silicon.

Acknowledgement

One of us (AKS) thanks the Department of Science and Technology, New Delhi, for financial support.

References

Batstone J L, Tischler M A and Collins R T 1993 *Appl. Phys. Lett.* **62** 2667
Bhat S V, Jayaram K, Muthu D V S and Sood A K 1992 *Proc. Solid State Phys. Symp.* **35-c** 198
Brandt M S, Fuchs H D, Stutzmann M, Weber J and Cardona M 1992 *Solid State Commun.* **81** 307
Buda F, Kohanoff J and Parrinello M 1992 *Phys. Rev. Lett.* **69** 1272
Campbell I H and Fauchet P M 1986 *Solid State Commun.* **58** 739
Canham L T 1990 *Appl. Phys. Lett.* **57** 1046
Cullis A J and Canham L T 1991 *Nature (London)* **353** 335
Deák P, Rosenbauer M, Stutzmann M, Weber J and Brandt M S 1992 *Phys. Rev. Lett.* **69** 2531
Friedersdorf L E, Searson P C, Prokes S M, Glembocki O J and Macaulay J M 1992 *Appl. Phys. Lett.* **60** 2285
Fuchs H D, Stutzmann M, Brandt M S, Rosenbauer M, Weber J, Breitschwerdt A, Deák P and Cardona M 1993 *Phys. Rev.* **B48** 8172
Iqbal Z and Vepřek S 1982 *J. Phys. C:Solid State Phys.* **15** 377
Lee H -J *et al* 1993 *Appl. Phys. Lett.* **62** 855
Li K-H, Tsai C, Sarathy J and Campbell J C 1993 *Appl. Phys. Lett.* **62** 3192
Petrova-Koch V, Muschik T, Kux A, Meyer B K, Koch F and Lehmenn V 1992 *Appl. Phys. Lett.* **61** 943
Prokes S M, Carlos W E and Bermudez V M 1992 *Appl. Phys. Lett.* **61** 1447
Proot P, Delerue C and Allan G 1992 *Appl. Phys. Lett.* **61** 1948
Qin G G and Jia Y Q 1993 *Solid State Commun.* **86** 559
Read A J, Needs R J, Nash K J, Canham L T, Calcott P D J and Qteish A 1992 *Phys. Rev. Lett.* **69** 1232
Richter H, Wang Z P and Ley L 1981 *Solid State Commun.* **39** 625
Roy A, Chainani A, Sarma D D and Sood A K 1992 *Appl. Phys. Lett.* **61** 1655
Roy A, Jayaram K and Sood A K 1994 *Solid State Commun.* **89** 229
Shih S, Jung K H, Kwong D L, Kovar M and White J M 1993 *Appl. Phys. Lett.* **62** 1780
Sood A K, Jayaram K and Muthu D V S 1992 *J. Appl. Phys.* **72** 4963
Sui Z, Leong P P, Herman I P, Higashi G S and Temkin H 1992 *Appl. Phys. Lett.* **60** 2086
Tsu R, Shen H and Dutta M 1992 *Appl. Phys. Lett.* **60** 112
Uhlir A 1956 *Bell Syst. Tech J.* **35** 333
Vial C, Bsiesy A, Gaspard F, Hérino R, Ligeon M, Muller F, Romestain R and MacFarlane R M 1992 *Phys. Rev.* **B45** 14,171
Wang X, Huang D, Ye L, Yang M, Hao P, Fu H, Hou X and Xie X 1993 *Phys, Rev. Lett.* **71** 1265
Weng Y M, Fan Zh N and Zong X F 1993 *Appl. Phys. Lett.* **63** 168